Giant spin-accumulation signal and pure spin-current-induced reversible magnetization switching

TAO YANG[1], TAKASHI KIMURA[1,2] AND YOSHICHIKA OTANI[1,2]*

[1]Advanced Science Institute, RIKEN, 2-1 Hirosawa, Wako, Saitama 351-0198, Japan

[2]Institute for Solid State Physics, University of Tokyo, Kashiwa, Chiba 277-8581, Japan

*e-mail: yotani@issp.u-tokyo.ac.jp

Published online: 5 October 2008; doi:10.1038/nphys1095

A number of proposed next-generation electronic devices, including novel memory elements[1] and versatile transistor circuits[2], rely on spin currents, that is, the flow of electron angular momentum. A spin current may interact with a magnetic nanostructure and give rise to spin-dependent transport phenomena, or excite magnetization dynamics[1–11]. In contrast to a spin-polarized charge current, a pure spin current does not produce any charge-related spurious effects[12,13]. One way to produce a pure spin current is non-local electrical-spin injection[12–18], but this approach has suffered so far from low injection efficiency. Here, we demonstrate a significant enhancement of the non-local injection efficiency in a lateral spin valve prepared with an entirely *in situ* fabrication process. Improvements to the interface quality and the device structure lead to an increase of the spin-signal amplitude by an order of magnitude. The generated pure spin current enables the magnetization reversal of a nanomagnet with the same efficiency as in the case of using charge currents. These results are important for further theoretical developments in multi-terminal structures[2], but also with a view towards realizing novel devices driven by pure spin currents.

In a vertical spin-valve nanopillar consisting of a ferromagnet/non-magnet/ferromagnet trilayer, the magnetic state can be switched between the antiparallel and the parallel configurations by applying a charge current[1–11]. This charge-current-induced magnetization switching (CIMS) is the result of a direct transfer of spin angular momentum from the spin current carried along the charge current to the localized magnetic moment in the ferromagnet. Separation of the charge and spin components raises the possibility of chargeless pure spin-current-induced magnetization switching (pure spin CIMS).

The pure spin current transfers only spin angular momentum, and thus provides an attractive means to manipulate the magnetic state in magnetic nanostructures as well as a quiet electrical background for experimental studies. The pure spin current I_S can be generated by the diffusion of the accumulated spins[12–20] in a metallic lateral spin-valve (LSV) structure with non-local electrical spin injection, as shown in Fig. 1a. When the spin accumulation at the interface between the permalloy (Py) and Cu wires on the detector side is non-collinear to the Py magnetization, the transverse component of the pure spin

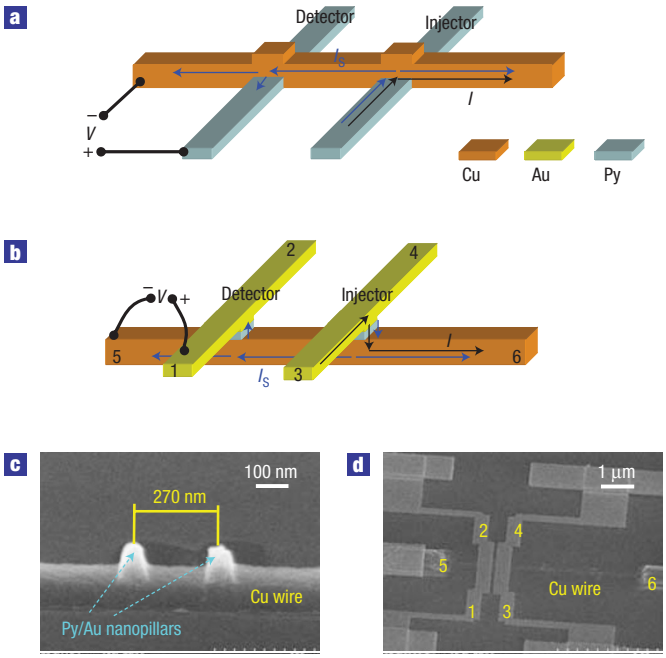

Figure 1 Sample structure. a, Schematic structure of a typical previously reported LSV. **b**, Schematic structure of our present LSV. **c**, Scanning electron micrograph taken during fabrication, showing a Cu wire with two Py/Au nanopillars. **d**, Scanning electron micrograph of the finished sample. The non-local measurement geometry is also shown in **a** and **b**, with I being the charge current and I_S being the spin current. For the sample shown in **c** and **d**, the Py nanomagnets in both the detector and the injector nanopillars are 20 nm in thickness. The Cu wire is 170 nm in width and 65 nm in thickness. The in-plane sizes of the two rectangular Py nanomagnets are $80 \times 170\,nm^2$ and $75 \times 170\,nm^2$ respectively, and their long axes are perpendicular to the Cu wire. The spins injected from the Py into the Cu are accumulated at the interface and diffuse, which creates a pure spin current flowing in the Cu wire and into the detector. Spin-dependent conduction in the detector nanomagnet leads to a difference in the electrochemical potential between the Py and Cu terminals. Therefore, a voltage V is measured, which is proportional to the spin accumulation at the Cu/detector interface[15].

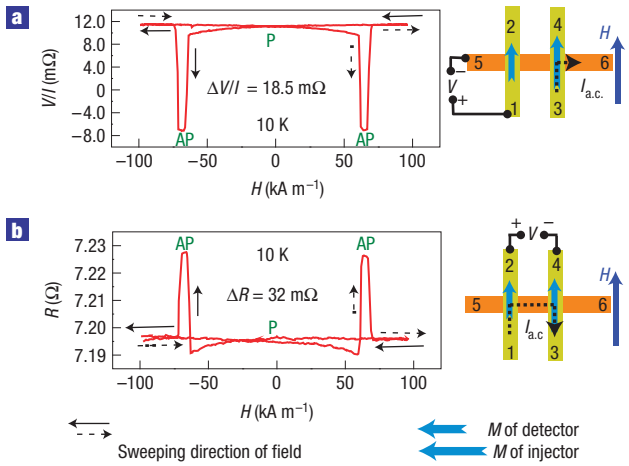

Figure 2 Transport measurement results for the sample shown in Fig. 1c,d. **a**, Non-local spin-valve signal as a function of magnetic field. **b**, Local spin-valve signal as a function of magnetic field. AP: antiparallel; P: parallel. The measurement geometry is drawn beside each graph.

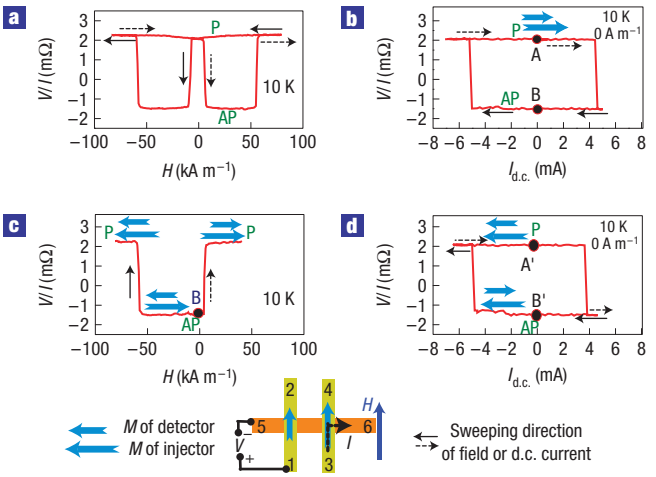

Figure 3 Non-local spin injection results for a sample with 4-nm-thick Py nanomagnet in the detector. **a**, Non-local spin-valve signal as a function of magnetic field. **b**, The non-local spin signal as a function of injected d.c. current. The loop starts at the initial parallel state A. **c**, The dependence of non-local spin-valve signal on the magnetic field for the antiparallel state B shown in **b**. **d**, The same measurement as **b**, but with an opposite initial parallel state A′. The measurement geometry is drawn below the graphs.

current is absorbed on entering the detector. Therefore, in the absence of a charge current, a spin-transfer torque could still be exerted on the Py magnetization[2,18]. However, so far, reversible magnetic switching similar to the CIMS has not been achieved by using pure spin currents, mainly because of low spin-injection efficiency. Usually the LSV is fabricated through two separate processes for the ferromagnet and the non-magnet nanowires, which inevitably introduces contamination or oxidation at the ferromagnet/non-magnet interfaces, causing spin-flip scattering and leading to the loss of the spin signal.

To improve the non-local spin injection efficiency, we have fabricated the newly designed sample shown in Fig. 1b. The injector and the detector are not nanowires but Py($Ni_{81}Fe_{19}$)/Au nanopillars whose constituents (Cu, Py and Au) are all deposited successively in the same vacuum, yielding very clean interfaces. The measured non-local spin-valve signal V/I is plotted in Fig. 2a as a function of the magnetic field applied along the easy axis of the Py nanomagnets. The sharp transitions in the non-local spin-valve signal correspond to the magnetic switching of the Py nanomagnets. The higher and the lower values of the non-local spin-valve signal correspond to the parallel and antiparallel states respectively. The difference in the non-local spin-valve signal $\Delta V/I$ between antiparallel and parallel states is proportional to the spin accumulation in the Cu wire. The observed $\Delta V/I$ signal is surprisingly large, ranging from 8 to 21 mΩ at 10 K for ten samples fabricated in two batches. At room temperature, $\Delta V/I$ is reduced to approximately 1/3 of its value at 10 K. These values are an order of magnitude larger than previously reported values in Py/Cu LSVs with the same injector-to-detector separation[12,13,15,16]. The giant non-local spin-valve signal indicates that giant spin accumulation takes place in the Cu wire, demonstrating high non-local spin injection efficiency. The main reason for this large signal is the improved interface quality between the Py and Cu, which minimizes the interfacial spin-flip scattering that causes a suppression of the spin signal. By solving the spin-diffusion equation[21,22], the non-local spin signal is analytically deduced as[20]

$$\frac{\Delta V}{I} = \frac{P_{Py}^2 R_{SPy}^2}{2R_{SPy}\exp(d/\lambda_{Cu}) + R_{SCu}\sinh(d/\lambda_{Cu})}, \qquad (1)$$

where P, λ and d are respectively the spin polarization factor, the spin-diffusion length and the centre-to-centre distance between the injector and detector, that is, the 270-nm distance shown in Fig. 1c. R_S is the spin resistance, defined as $R_S = 2\rho\lambda/[(1-P^2)S]$, with the resistivity ρ and the effective cross-sectional area S. Using the materials parameters determined in our recent experiments[20], including the spin-diffusion lengths of 1,000 nm and 5 nm for Cu and Py respectively, $\Delta V/I$ is calculated as being 14.4 mΩ for the sample shown in Fig. 1c,d. Despite some sample-to-sample variation, the experimental results are in good agreement with the theoretical calculation.

According to equation (1), a large value of S causes a reduction of the non-local spin-valve signal $\Delta V/I$. Because of the short spin-diffusion length of ∼5 nm, S is the Cu/Py-interface area for Py. As shown in Fig. 1b, in our present structure, S is effectively diminished. In addition, the inhomogeneous spin current distribution observed in our previous LSVs (ref. 15) should be diminished in the present structure. Therefore, in addition to the clean interfaces, our particular structure also contributes to the improved non-local spin signal.

For comparison, the local spin-valve signal measured between contacts 2 and 4 by applying the current between contacts 1 and 3 is shown in Fig. 2b. The anisotropic magneto-resistance effect is visible in the curve. The resistance difference between the antiparallel and parallel states is 32 mΩ, 1.7 times larger than the non-local spin signal, in reasonable agreement with the factor of 2 predicted in ref. 13.

With the benefit of the highly improved non-local spin injection efficiency, we now study magnetization switching induced by a pure spin current. Because the spin transfer occurs near the interface[1,23], we reduce the Py thickness of the detector to 4 nm to minimize the spin current necessary for the magnetization switching. Figure 3a shows the non-local spin-valve signal as a function of the external field for such a sample. The values of $\Delta V/I$ for these samples are around 4 mΩ, smaller than that in Fig. 2a, but still much larger than previously reported values. The lower non-local spin-valve signal is attributed to the fact that the Py thickness is reduced

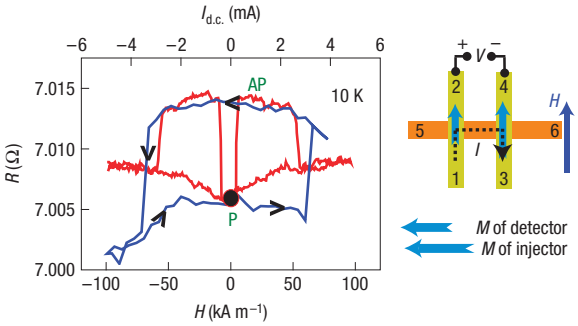

Figure 4 Local spin injection results for the sample described in Fig. 3. The red line is the field dependence; the blue line is the d.c. current dependence.

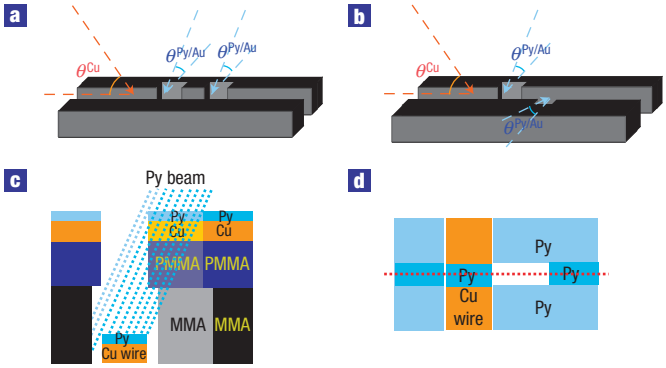

Figure 5 Illustrations of electron beam lithography and oblique deposition. **a**, Schematic diagram of the pattered resist for the oblique deposition of the sample in Fig. 2. **b**, Schematic diagram of the pattered resist for the oblique deposition of the sample in Fig. 3. **c**, Cross-section depiction of the deposition of the nanopillar. **d**, Top view of **c**. The dotted red line indicates the position of the cross-section. The deeper colour for the same material corresponds to the cross-section plane.

and is comparable to the spin-diffusion length. This decreases the difference in the electrochemical potential between the detector and the Cu wire[15]. By comparison with the anisotropic magnetoresistance measurements for both the detector and the injector, the higher and lower values of the switching fields are identified as being the switching fields of the Py injector and detector nanomagnets, respectively.

A variable d.c. current is applied between contacts 3 and 6. The sample is preset to a parallel state (denoted A in Fig. 3) at which both magnetizations are aligned in the positive field direction. As can be seen in Fig. 3b, as the d.c. current is increased, the non-local spin-valve signal sharply decreases at about 4.5 mA, indicating a clear magnetization reversal. According to the change in the non-local spin-valve signal, the parallel state is transformed into an antiparallel state (denoted B), which is switched back to the parallel state by a negative d.c. current of −5 mA. Therefore, reversible magnetization switching between antiparallel and parallel states is realized by means of non-local spin injection. Similar results are also observed for other samples.

The magnetic configuration of the antiparallel state B is characterized by applying an external field in either the positive or negative direction. According to the switching-field values shown in Fig. 3c, the magnetic configuration of the antiparallel state B is easily determined, as shown in the figure. The switch from the initial parallel state A to the antiparallel state B is realized by the reversal of the detector magnetization. Therefore, a charge current between contacts 3 and 6 induces switching of the detector magnetization, where there is no charge current. The switching from the antiparallel back to the parallel states is also confirmed to take place through the reversal of the detector magnetization.

As shown in Fig. 3d, for an initial parallel state oriented in the opposite direction, A′, a similar switching loop is measured. In Fig. 3b,d, regardless of the magnetization orientation of the initial parallel state, the parallel-to-antiparallel switching is caused by a positive d.c. current and the antiparallel-to-parallel switching by a negative d.c. current, indicating that the Oersted field hardly affects the magnetization switching. This relationship between the d.c. current direction and the switching direction can be explained only by the spin-transfer theory. Therefore, the current-induced magnetization reversals in Fig. 3b,d are induced by the spin transfer from the pure spin current generated in the non-local geometry, as shown in Fig. 1.

The spin current I_S flowing into the detector can be derived from the spin-diffusion equation as

$$I_S = \frac{(\Delta V/I)I_{d.c.}}{R_{SPy}P_{Py}} \frac{(1+R_{SPy}/R_{SAu})e^{t/\lambda_{Py}} - (1-R_{SPy}/R_{SAu})e^{-t/\lambda_{Py}}}{(1+R_{SPy}/R_{SAu})e^{t/\lambda_{Py}} + (1-R_{SPy}/R_{SAu})e^{-t/\lambda_{Py}} - 2},$$

with t being the Py thickness of the detector. Using our observed critical switching d.c. current of 5 mA, we calculate the critical spin current for magnetization switching as 317 μA, which is equivalent to a spin current density of approximately 2.5×10^{10} A m^{-2}.

When there is a small angle θ between the injector and detector magnetizations, the transverse component $(\hbar/2)(I_S/e)\sin\theta$ of the angular momentum carried by the spin current is transferred to the detector. By putting this contribution into the Landau–Lifschitz–Gilbert equation and neglecting the small in-plane uniaxial anisotropy, the critical spin current for the switching between the antiparallel and parallel states is derived as[7]

$$I_S = \frac{\alpha e M^2 V_{vol} \mu_0}{\hbar}.$$

Here α is the damping factor, M is the magnetization, V_{vol} is the volume of the Py nanomagnet in the detector and μ_0 is the permeability in vacuum. For Py, α is reported as being between 0.002 and 0.007 (refs 24–26). By taking $M = 7.8 \times 10^5$ A m^{-1}, the critical spin current density for the switching is calculated as being in the range of 1–3.5×10^{10} A m^{-2}, in very good agreement with the estimate from our experimental data. On the other hand, in the previous CIMS experiments, the critical switching charge current density for Py/Cu/Py nanopillars[10,27,28] was reported in the range 1×10^{11}–3×10^{11} A m^{-2}. With a current polarization of ~0.2, the critical local spin current density for the switching in the CIMS experiments is in the range 2–6×10^{10} A m^{-2}. Therefore, our results are theoretically reasonable, and consistent with the reported CIMS results.

Compared with the Cu spacer thickness in a Py/Cu/Py nanopillar used in the CIMS experiment, which is usually less than 10 nm, the distance d of 270 nm between injector and detector in our sample seems very large. However, because of the long spin-diffusion length of 1,000 nm, the spin signal loss after travelling 270 nm in the Cu wire is only $1 - \exp(-270/1{,}000) = 24\%$. Thus, 3/4 of the spin signal, the polarized spin angular momentum, remains. In addition, direct local-injection experiments using the same sample also bring about the CIMS (Fig. 4). This is complementary proof indicating the switching is induced by the spin-transfer effect over the length of 270 nm.

The realization of magnetization switching induced by both local and non-local spin injection unifies the up-to-now separate developments of perpendicular nanopillars and lateral magnetic nanostructures. Relative to the previous work[18], much more than the improvement in the fabrication process, the high non-local spin injection efficiency and the induced efficient magnetization switching are critical for verifying the theoretical work in these multi-terminal structures[2]. Obtained with the high-quality multi-terminal structure comprising laterally connected ferromagnetic nanopillars, our present results also confirm that it is possible to realize such novel multi-terminal spintronics devices as the spin-flip transistor and spin-torque transistor[2].

METHODS

FABRICATION

A special process was developed to fabricate samples with clean interfaces. First, the bilayer resist (250-nm-thick 8% methylmethacrylate (MMA)/150-nm-thick 4% polymethyl methacrylate (PMMA)) was patterned by electron beam lithography into the shapes shown in Fig. 5. Figure 5a shows the resist for the sample in Fig. 2 and Fig. 5b shows the resist for the sample in Fig. 3. Figure 5,c,d schematically shows the local edge profile of the pattered resist. Then the Cu wire was deposited at an angle θ^{Cu} (50° from the substrate surface), followed promptly by the deposition of Py/Au at an angle $\theta^{Py/Au}$ (60° from the substrate surface) in the same vacuum. For the sample in Fig. 2, detector and injector nanopillars were deposited simultaneously. For the sample in Fig. 3, injector and detector nanopillars were deposited one after the other. The deposition was carried out by electron beam evaporation in a base vacuum better than 1×10^{-7} Pa and a growth vacuum better than 2×10^{-6} Pa. The material purities are Cu 99.9999%, Py 99.95% and Au 99.9%. After the lift-off process, a Cu wire with two Py/Au nanopillars on it is formed as shown in Fig. 1c. Then Al_2O_3 was deposited perpendicularly to bury the Cu wire and part of the Py/Au nanopillars. Finally, the top contacts were formed by low-angle ion milling and the top electrodes were patterned by electron beam lithography and optical lithography.

TRANSPORT MEASUREMENTS

The transport measurements were carried out with a four-probe system. The lowest temperature was 10 K. The a.c. current in the non-local measurement was 250 μA in amplitude and 79 Hz in frequency. A lock-in amplifier was used to measure the output voltage. An in-plane magnetic field up to 4 kOe was applied. The non-local spin-injection-induced magnetization switching was measured by applying a d.c. current for 2 s, then removing the d.c. current and applying the a.c. current to measure the non-local spin-valve signal.

Received 10 March 2008; accepted 4 September 2008; published 5 October 2008.

References

1. Slonczewski, J. C. Current-driven excitation of magnetic multilayers. *J. Magn. Magn. Mater.* **159**, L1–L7 (1996).
2. Brataas, A., Bauer, G. E. W. & Kelly, P. J. Non-collinear magnetoelectronics. *Phys. Rep.* **427**, 157–255 (2006).
3. Berger, L. Emission of spin waves by a magnetic multilayer traversed by a current. *Phys. Rev. B* **54**, 9353–9358 (1996).
4. Tsoi, M *et al.* Excitation of a magnetic multilayer by an electric current. *Phys. Rev. Lett.* **80**, 4281–4284 (1998).
5. Myers, E. B., Ralph, D. C., Katine, J. A., Louie, R. N. & Buhrman, R. A. Current-induced switching of domains in magnetic multilayer devices. *Science* **285**, 867–870 (1999).
6. Wegrowe, J.-E., Kelly, D., Jaccard, Y., Guittienne, Ph. & Ansermet, J.-Ph. Current-induced magnetization reversal in magnetic nanowires. *Europhys. Lett.* **45**, 626–632 (1999).
7. Sun, J. Z. Spin-current interaction with a monodomain magnetic body: A model study. *Phys. Rev. B* **62**, 570–578 (2000).
8. Katine, J. A., Albert, F. J., Buhrman, R. A., Myers, E. B. & Ralph, D. C. Current-driven magnetization reversal and spin-wave excitations in Co/Cu/Co pillars. *Phys. Rev. Lett.* **84**, 3149–3152 (2000).
9. Grollier, J. H. *et al.* Spin-polarized current induced switching in Co/Cu/Co pillars. *Appl. Phys. Lett.* **78**, 3663–3665 (2001).
10. Urazhdin, S. Current-driven magnetic excitations in permalloy-based multilayer nanopillars. *Phys. Rev. Lett.* **91**, 146803 (2003).
11. Jiang, Y. *et al.* Effective reduction of critical current for current-induced magnetization switching by a Ru layer insertion in an exchange-biased spin valve. *Phys. Rev. Lett.* **92**, 167204 (2004).
12. Jedema, F. J., Filip, A. T. & van Wees, B. J. Electrical spin injection and accumulation at room temperature in an all-metal mesoscopic spin valve. *Nature* **410**, 345–348 (2001).
13. Jedema, F. J., Nijboer, M. S., Filip, A. T. & van Wees, B. J. Spin injection and spin accumulation in all-metal mesoscopic spin valves. *Phys. Rev. B* **67**, 085319 (2003).
14. Johnson, M. & Silsbee, R. H. Interfacial charge-spin coupling: Injection and detection of spin magnetization in metals. *Phys. Rev. Lett.* **55**, 1790–1793 (1985).
15. Kimura, T. & Otani, Y. Spin transport in lateral ferromagnetic/nonmagnetic hybrid structures. *J. Phys. Condens. Matter* **19**, 165216 (2007).
16. Kimura, T., Hamrle, J., Otani, Y., Tsukagoshi, K. & Aoyagi, Y. Spin-dependent boundary resistance in the lateral spin-valve structure. *Appl. Phys. Lett.* **85**, 3501–3503 (2004).
17. Garzon, S., Žutić, I. & Webb, R. A. Temperature-dependent asymmetry of the nonlocal spin-injection resistance: Evidence for spin nonconserving interface scattering. *Phys. Rev. Lett.* **94**, 176601 (2005).
18. Kimura, T., Otani, Y. & Hamrle, J. Switching magnetization of nanoscale ferromagnetic particle using nonlocal spin injection. *Phys. Rev. Lett.* **96**, 037201 (2006).
19. Kimura, T. & Otani, Y. Large spin accumulation in a permalloy-silver lateral spin valve. *Phys. Rev. Lett.* **99**, 196604 (2007).
20. Kimura, T., Sato, T. & Otani, Y. Temperature evolution of spin relaxation in NiFe/Cu lateral spin valve. *Phys. Rev. Lett.* **100**, 066602 (2008).
21. van Son, P. C., van Kempen, H. & Wyder, P. Boundary resistance of the ferromagnetic–nonferromagnetic metal interface. *Phys. Rev. Lett.* **58**, 2271–2273 (1987).
22. Valet, T. & Fert, A. Theory of the perpendicular magnetoresistance in magnetic multilayers. *Phys. Rev. B* **48**, 7099–7113 (1993).
23. Zhang, J. W., Levy, P. M., Zhang, S. F. & Antropov, V. Identification of transverse spin currents in noncollinear magnetic structures. *Phys. Rev. Lett.* **93**, 256602 (2004).
24. Kalarickal, S. S. *et al.* Ferromagnetic resonance linewidth in metallic thin films: Comparison of measurement methods. *J. Appl. Phys.* **99**, 093909 (2006).
25. Mircea, D. I. & Clinton, T. W. Near-field microwave probe for local ferromagnetic resonance characterization. *Appl. Phys. Lett.* **90**, 142504 (2007).
26. Olson, H. M., Krivosik, P., Srinivasan, K. & Patton, C. E. Ferromagnetic resonance. saturation and second order Suhl spin wave instability processes in thin permalloy films. *J. Appl. Phys.* **102**, 023904 (2007).
27. Krivorotov, I. N. *et al.* Time-domain measurements of nanomagnet dynamics driven by spin-transfer torques. *Science* **307**, 228–231 (2005).
28. Kurt, H., Loloee, R., Pratt, W. P. Jr. & Bass, J. Current-induced magnetization switching in permalloy-based nanopillars with Cu, Ag, and Au. *J. Appl. Phys.* **97**, 10C706 (2005).

Acknowledgements

Helpful discussions with J.-B. Laloë as well as his efforts to improve the English of this manuscript are gratefully acknowledged. We also thank K. Ito for useful discussions. This work was supported by a Grant-in-Aid for Scientific Research in Priority Area 'Creation and control of spin current' (19048013) from the Ministry of Education, Culture, Sports, Science and Technology, Japan.

Author contributions

Y.O. planned the project. T.Y. and T.K. carried out the experimental work and data analysis.

Author information

Reprints and permissions information is available online at http://npg.nature.com/reprintsandpermissions. Correspondence and requests for materials should be addressed to Y.O.